Revision 4

A Possible New Al-bearing Hydrous Mg-silicate (23 Å phase) in the Deep Upper Mantle

Nao CAI[1*], Toru INOUE[1], Kiyoshi FUJINO[1], Hiroaki OHFUJI[1], Hisayoshi YURIMOTO[2]

[1]Geodynamics Research Center, Ehime University, Matsuyama 790-8577, Japan

[2]Natural History Sciences, Hokkaido University, Sapporo 060-0810, Japan

*Corresponding author

Nao Cai

E-mail: nao@sci.ehime-u.ac.jp

Abstract

A new Al-bearing hydrous Mg-silicate which we named as **23** Å phase was synthesized at 10 GPa and 1000ºC, while also coexisting with diaspore and pyrope in the following system: phase A ($Mg_7Si_2O_8(OH)_6$) + Al_2O_3 + H_2O. The chemical composition of this new **23** Å phase is $Mg_{11}Al_2Si_4O_{16}(OH)_{12}$, and it contains about 12.1 wt% water. Powder X-ray diffraction and electron diffraction patterns show that this new **23** Å phase has a hexagonal structure, with a = 5.1972(2) Å, c = 22.991(4) Å, and V = 537.8(2) Å^3, and the possible space group is $P\bar{6}c2$, $P6_3cm$, or $P6_3/mcm$. The calculated density is 2.761 g/cm^3 accordingly, which was determined by assuming that the formula unit per cell (Z) is 1. This crystal structure is quite unique among mantle minerals in having an extraordinarily long c axis. Several experiments revealed that its stability region is very similar to that of phase A. We further confirmed that this new **23** Å phase was stable in the chlorite composition at 10 GPa and 1000ºC. The present results indicate that this new **23** Å hydrous phase will form in an Al-bearing subducting slab, and transport water together with Al into the deep upper mantle or even into the upper part of the transition zone.

Keywords: New hydrous Mg-silicate, **23** Å phase, phase A, chlorite, subduction zone, upper mantle.

Introduction

Water plays an important role in the deep mantle, as it influences the melting temperature (e.g., Inoue, 1994), nature of seismic discontinuities (e.g., Higo et al., 2001; Chen et al., 2002; Chen et al., 2011), mineral composition of the mantle (e.g., Kanzaki, 1991; Ohtani et al., 1995; Frost and Fei, 1998), etc. A recently reported study has shown that, despite the dry upper mantle (Saal et al., 2002), the mantle transition zone is indeed hydrous, with a water content of about 1.5 weight percent in ringwoodite (Pearson et al., 2014). Water may be transported into the mantle transition zone or deeper by subducted slabs in the form of dense hydrous magnesium silicates (DHMS) (Ohtani et al., 2001), as well as nominally anhydrous phases, such as pyroxene, olivine, and garnet.

Nowadays the MgO-SiO_2-H_2O (MSH) system is well defined, and it derives several hydrous minerals such as the alphabet phases A, B, superhydrous B (C), D (F, G), H (Ringwood and Major, 1967; Yamamoto and Akimoto, 1974; Akaogi and Akimoto, 1980; Liu, 1987; Kanzaki, 1991; Gasparik, 1993; Kudoh et al., 1993; Ohtani et al., 1997; Nishi et al., 2014), 10 Å phase, chondrodite, humite (Yamamoto and Akimoto, 1977), hydrous wadsleyite, and ringwoodite (Inoue et al., 1995, Inoue et al., 1998). These phases can be formed by the decomposition of antigorite (Irifune et al., 1998; Komabayashi et al., 2005) as the cold slab descends, which provides a way for water to enter into the deep Earth. Furthermore, in the sediment and mid-ocean ridge basalt compositions several hydrous phases like phase egg (Eggleton

et al., 1978), δ-AlOOH (Suzuki et al., 2000), topaz-OH (e.g. Wunder et al., 1993), lawsonite (e.g. Pawley et al., 1994; Okamoto and Maruyama, 1999), zoisite (e.g. Schmidt and Poli, 1994), and phengite (e.g. Domanik and Holloway, 1996) are also well recognized.

However, few researches have been done to clarify the phase relations in the MgO-Al_2O_3-SiO_2-H_2O (MASH) system, which should also be an important system for the deep Earth. The hydrous minerals involving the MASH composition include mhlorite, MgMgAl-pumpellyite (Fockenberg, 1998; Artioli et al., 1999), later identified as Mg-sursassite (Bromiley and Pawley, 2002; Gottschalk et al., 2000), Mg-chloritoid, and Mg-carpholite (Chopin and Schreyer, 1983), a recently reported hydrous Al-bearing pyroxene (HAPY, Gemmi et al., 2011), etc.

Previous studies (e.g. Rauch and Keppler, 2002; Litasov et al., 2007; Mierdel et al., 2007; Sakurai et al., 2014) have shown that Al can be incorporated into the structures of some hydrous and anhydrous phases, which, for example, can be expressed as $2Mg^{2+} = Al^{3+} + H^{+}$ or $Si^{4+} = Al^{3+} + H^{+}$. The water content increases with increasing Al in the structures.

In the present study, we conducted experiments on the Al incorporation into phase A, where Mg is 6-coordinated and Si is 4-coordinated (Horiuchi, et al., 1983). By trying to increase the water content through the substitution of Al^{3+} and H^{+} for Si^{4+} and/or $2Mg^{2+}$ in phase A, we encountered a new hydrous phase with a significant amount of Al, which has an unknown X-ray powder diffraction pattern. We

65 successfully obtained the cell parameters and chemical composition of this new phase by means of X-ray
66 diffraction (XRD), transmission electron microscopy (TEM), electron probe microanalysis (EPMA)
67 (energy or wavelength dispersive X-ray spectroscopy (EDS or WDS)), and secondary ion mass
68 spectrometry (SIMS). The phase transformations of chlorite have also been studied, in order to clarify
69 the existence of this new phase in the Al bearing composition along subducting slabs.

70 ## Experimental procedure

71 High pressure and high temperature experiments were conducted using a Kawai type 2000 ton
72 multi-anvil apparatus established at the Geodynamic Research Center (GRC) of Ehime University.
73 Tungsten carbide cubes with a truncated edge length of 8 mm and Co doped MgO octahedron with an
74 edge length of 14 mm were adopted as the second stage anvils and pressure medium, respectively. A
75 cylindrical graphite sleeve was used as a heater, and the temperature was monitored using a
76 W3%Re-W25%Re thermocouple. The cell assembly is shown in Fig. 1.

77 For Al incorporation experiments, two starting materials were prepared, and they are called S1 and
78 S2 throughout this paper. S1 was the mixture of $Al(OH)_3$, Al_2O_3, and synthesized phase A
79 ($Mg_7Si_2O_8(OH)_6$) with the molar ratio 1:1:1, and S2 was the mixture of MgO, $Mg(OH)_2$, SiO_2, Al_2O_3,
80 and $Al(OH)_3$ with the same chemical composition to S1. Both mixtures were crushed to less than ~1 μm
81 grain size and preserved in a drying oven. In a typical run under 10 GPa and 1000ºC, two Au or Pt

82 capsules with two mixtures were loaded into the MgO sleeve, which was surrounded by the graphite
83 heater. We prepared one more starting material named Syn for the synthesis experiment of this new
84 hydrous phase, which has a composition of $Mg_{5.7}AlSi_{1.9}O_8(OH)_6$. The decomposition experiments on
85 natural chlorite were also carried out at the same P-T condition.

86 The recovered run products were sliced, polished, and then carbon coated to perform the chemical
87 composition measurement, using EPMA (JEOL JSM-6510LV for EDS or JEOL 8800 for WDS) for
88 MgO-Al_2O_3-SiO_2 components at Ehime University. The water content was measured by a SIMS
89 (CAMECA IMS-6f) installed at Hokkaido University, using a natural amphibole crystal as a standard
90 (1.66 wt% of H_2O. Miyagi and Yurimoto, 1995). In addition, San Carlos olivine was used for the
91 background H intensities, due to its low H concentration (10–60 ppm. Kurosawa et al., 1997).

92 The X-ray diffraction patterns of this new phase were obtained using a Micro-focused diffractometer
93 (Rigaku MicroMax-007HF) and a powder X-ray diffractometer (Rigaku UltimaIV/DD).
94 Monochromatized CuKα1 radiation was employed. For the TEM analysis, the recovered samples were
95 Ar ion-thinned by an Ion Slicer (JEOL EM-09100 IS) at 3–5.5 kV, 7–20 μA, and glancing angle of 0–5º.
96 These thin specimens were observed by TEM (JEOL JEM-2010) operating at 200 kV at the GRC, Ehime
97 University. A two axis-tilting holder was used to obtain the selected-area-electron-diffraction (SAED)
98 patterns and the transmitted images. The SAED patterns and the transmitted images were recorded by a

CCD detector.

Results and discussion

The new hydrous Mg-silicate was observed to coexist with pyrope ($Mg_3Al_2Si_3O_{12}$) and diaspore (AlOOH) in the phase A ($Mg_7Si_2O_8(OH)_6$) + Al_2O_3 + H_2O system. In sample S1 a small amount of phase A ($Mg_7Si_2O_8(OH)_6$) and spinel ($MgAl_2O_4$) existed in the low temperature zone. This may be due to a temperature gradient. In sample S2 no phase A or spinel was observed. In both samples there were some minor phases (<5% in volume) such as brucite ($Mg(OH)_2$) and gibbsite ($Al(OH)_3$) in the low temperature zone, and we regarded these phases as disequilibrium products. The chemical compositions of the new phase and its coexisting phases, which were measured by EPMA (EDS) and SIMS, are listed in Table 1 and shown in the ternary diagram in Fig. 2. For the EPMA measurements we noticed that the pyrope had a slightly high Mg content and low Si content compared with $Mg_3Al_2Si_3O_{12}$. The Mg/Si ratios of pyrope in sample S1 and S2 equal to 1.08(1) and 1.05(1), respectively. While we have carefully checked the standards (e.g. En and Ky in Table 1) before measuring our samples, the composition deviation may be caused by the OH component in the pyrope structure, with a possible substitution of $4H^+$ for Si^{4+}. The chemical composition of the new phase was estimated to be $Mg_{5.7}AlSi_{1.9}O_8(OH)_6$. Due to the poor crystal qualities of new phase and diaspore, their compositions may be a little different from the stoichiometry.

Almost pure sample of the new phase with relatively high crystal quality was successfully synthesized in subsequent experiment under 10 GPa and 1000ºC, using $Mg_{5.7}AlSi_{1.9}O_8(OH)_6$ as the starting composition. A small amount of pyrope existed in the high temperature zone in the run product. The chemical compositions of both the new phase and pyrope were analyzed by EPMA (WDS) and SIMS and are listed in Table 1, which reveals that this new hydrous Mg-silicate has a chemical composition close to $Mg_{11}Al_2Si_4O_{16}(OH)_{12}$. The calculated ideal water content for this composition is 12.1%, which is very close to that of phase A (11.8%). Under the microscope this new phase had a plate-like shape, with the thickness of several micrometers. This crystal shape may have some effects on measuring the composition. Actually we have conducted several experiments on different pressure and temperature (i.e. 6 - 12 GPa, 700 - 1000ºC) conditions to confirm this composition. No clear dependences on pressure and/or temperature were observed in the composition of this new phase. The measured compositions were slightly scattering, with the Mg/Si ratios changing from 2.65 to 2.80, and Al/Si ratios from 0.49 to 0.51. The composition deviates may be due to the cracks, grain boundaries, or the measurement error. Thus we assume that this new phase has an ideal chemical composition given by $Mg_{11}Al_2Si_4O_{16}(OH)_{12,}$ which has the Mg/Si and Al/Si ratios equal to 2.75 and 0.5, respectively.

The XRD pattern (Fig. 3) for this new phase is very different from those of phase A and any other hydrous or anhydrous phases. In order to derive its structure information, several electron diffraction

patterns were obtained using TEM (Fig. 4).

Fig. 4a illustrates the SAED pattern of the new hydrous phase showing that this reciprocal lattice plane has hexagonal symmetry, and the other SAED patterns (Fig. 4b&e) show that the reciprocal lattice of this new phase has spots with a very short distance perpendicular to the plane of hexagonal symmetry. Further SAED patterns of the new hydrous phase reveal that all the diffraction spots can be indexed by the hexagonal lattice with the cell parameters a = 5.23(6) Å, c = 23.2(2) Å. At this stage, there still remains a possibility that this lattice may be hexagonal or trigonal. However, existence of the mirror planes perpendicular to both [100]* and [110]* (Fig. 4c and d) excludes the possibility of a trigonal system because in the trigonal system mirror planes perpendicular to both [100]* and [110]* are not possible. Besides, these diffraction spots have the extinction rule that l = 2n +1 (n = integer) is extinct only for $h0l$ (equivalent to $h\bar{h}l$) spots (Fig. 4b and e). Based on this extinction rule, the possible space group of the new hydrous phase is constrained to be $P\bar{6}c2$, $P6_3cm$, or $P6_3/mcm$ in hexagonal structures. The $h0l$ spots with h = 3n + 1 and 3n + 2 (n = integer) are characterized by strong diffuseness (Fig. 4e), indicating some defects in the structure, which will be discussed in a separate paper.

According to the above information the powder diffraction pattern was successfully indexed with the lattice parameters a = 5.1972(2) Å, c = 22.991(4) Å, and V = 537.8(2) Å^3. The result is shown in Figure 3, and the observed and calculated d-spacings for this new phase are listed in Table 2. This ~**23** Å

elongated c-axis is characteristic in this phase, so here we name this new hydrous phase as "**23** Å phase". There are some weak peaks representing 1 0 7, 1 0 9 and 2 0 7 of the new **23** Å phase, which should be extinct by the extinction rules. Since in electron diffraction patterns *h*0*l* spots (h ≠ 3n) always show heavy streaking (Fig. 4e), this may also reflect in the powder diffraction, and hence cause the existence of *h*0*l* (h ≠ 3n, *l* = 2n + 1) peaks. There are still some unidentified peaks at 2θ of about 20.83°, 26.67° and 32.72°, we consider that those peaks do not belong to the new **23** Å phase, as there are no such peaks in the micro-focus X-ray diffraction patterns. We are now conducting the single crystal X-ray diffraction measurement. The result will be discussed in a separate paper.

If we assume that the formula unit per cell (Z) equals 1, the calculated density for this new **23** Å phase (12.1 wt% H_2O, 2.761 g/cm^3) is similar or slightly higher than those of clinochlore (12 wt% H_2O, 2.65 g/cm^3), talc (4.7 wt% H_2O, 2.75 g/cm^3), and phase E (16.9 wt% H_2O, 2.88 g/cm^3) considering the water contents. However, compared to the other dense hydrous magnesium silicates, such as phase A (11.8 wt% H_2O, 2.96 g/cm^3), phase B (2.4 wt% H_2O, 3.37 g/cm^3), superhydrous phase B (5.8 wt% H_2O, 3.33 g/cm^3), and phase D (17.6 wt% H_2O, 3.50 g/cm^3), the density of this new **23** Å phase is slightly lower. It is also lower than that of phase HAPY (7 wt% H_2O, 3.14 g/cm^3).

Several experiments have been conducted in order to identify the stability region of this new **23** Å Mg-silicate. As shown in Fig. 5, this new **23** Å phase is stable up to 12 GPa and 1000ºC, which is very

similar to the P, T stability region of phase A (Wunder, 1998), and along the cold slab condition, it can survive until it reaches the transition zone. At higher pressures it breaks down into Al-bearing superhydrous phase B ($(Mg_{9.6}Al_{0.4})(Si_{2.6}Al_{0.4})O_{14}(OH)_4$), Al-bearing phase E (Nonstoichiometric, confirmed by XRD), pyrope, and fluid, while at lower pressures it breaks down into chondrodite, pyrope, forsterite, and fluid. This means that this new **23** Å phase can transport H_2O into the deep upper mantle, even into the upper part of the transition zone.

Implications

In the Mg-end antigorite composition ($Mg_3Si_2O_5(OH)_4$), along the cold slab condition, phase A is possibly the dominant hydrous phase ~~in the whole upper mantle~~ (Irifune et al., 1998; Komabayashi et al., 2005). Since a significant amount of aluminum also exists in a real subduction environment, it is reasonable to suppose that aluminum bearing hydrous minerals will form during the metamorphism of minerals such as chlorite [$(Mg_5Al)(AlSi_3)O_{10}(OH)_8$]]. In such an Al-bearing situation we predict that this new **23** Å phase will form and become the dominant hydrous phase beyond the stability region of chlorite along the subducting slab, as the present study shows that phase A can easily react with Al^{3+} and produce this new **23** Å phase. ~~Thus, it is necessary to clarify the stability of this new **23** Å phase in something related to a real mantle composition, such as chlorite.~~ Accordingly, a decomposition experiment on natural chlorite, an important constituent of a metamorphosed mantle in an Al-bearing

system, was conducted at 10 GPa and 1000ºC to confirm the appearance of the **23** Å phase. The result showed that the chlorite decomposes into pyrope, chondrodite, the new **23** Å phase, phase A, and fluids (Fig. 6), suggesting that along the cold slab the **23** Å phase can coexist with phase A in an Al-bearing mantle composition. Thus, this new Al-bearing hydrous **23** Å phase should be an important hydrous phase together with phase A to transport water into the deep Earth. The present result of the coexisting new **23** Å phase and phase A shows that the amounts of these phases in the upper mantle depend on the bulk Al_2O_3 and H_2O contents.

Recently, phase HAPY was reported in the MASH system at 5.4 GPa and 720ºC (Gemini et al., 2011), but no phase HAPY was observed at 10 GPa and 1000ºC in the chlorite composition. We are further investigating the stability of this new **23** Å phase in the chlorite composition, especially just beyond the stability region of chlorite (Staudigel and Schreyer, 1977; Fockenberg, 1995). The results will be reported in a separate paper in the near future.

The discovery of this new hydrous **23** Å phase extends the stability region of the hydrous phase in the MASH system along the subduction zone. The stability region of this new **23** Å phase is similar to that of phase A. Thus, in the Al-bearing mantle composition, this new hydrous **23** Å phase should be an important water reservoir to transport water together with Al into the deep upper mantle, even into the transition zone.

Acknowledgements

This work was conducted as a part of a Ph. D. thesis of N. Cai at Ehime University. The authors would like to thank T. Shinmei for his great help in high-pressure experiments and electron microprobe observations. We also appreciate N. Sakamoto for the assistance in SIMS measurements at Hokkaido University, and Prof. T. Kuribayashi at Tohoku University for his great comments on this project. The research was supported by a Grant-in-Aid for Scientific Research (A) [KAKENHI] from the Japan Society for the Promotion of Science (JSPS) given to T. Inoue (No. 26247073).

References

Akaogi, M., and Akimoto, S-I. (1980) High-pressure stability of a dense hydrous magnesium silicate $Mg_{23}Si_8O_{42}H_6$ and some geophysical implications. Journal of geophysical research, 85, 6944–6948.

Angel, R.J., Frost, D.J., Ross, N.L., and Hemley, R. (2001) Stabilities and equations of state of dense hydrous magnesium silicates. Physics of the Earth and Planetary Interiors, 127, 181–196.

Artioli, G., Fumagalli, P., and Poli, S. (1999) The crystal structure of $Mg_8(Mg_2Al_2)Al_8Si_{12}(O,OH)_{56}$ pumpellyite and its relevance in ultramafic systems at high pressure. American Mineralogist, 84, 1906–1914.

Bromiley, G.D., and Pawley, A.R. (2002) The high-pressure stability of Mg-sursassite in a model hydrous peridotite: a possible mechanism for the deep subduction of significant volumes of H_2O. Contributions to Mineralogy and Petrology, 142, 714–723.

Chen, J., Inoue, T., Yurimoto, H., and Weidner, D.J. (2002) Effect of water on olivine-wadsleyite phase boundary in the $(Mg,Fe)_2SiO_4$ system. Geophysical Research Letters, 29, 1875.

Chen, J., Liu, H., and Girard, J. (2011) Comparative in situ X-ray diffraction study of San Carlos olivine: Influence of water on the 410 km seismic velocity jump in Earth's mantle. American Mineralogist, 96, 697-702.

Chopin, C., and Schreyer, W. (1983) Magnesiocarpholite and magnesiochloritoid: two index minerals of

pelitic blueschists and their preliminary phase relations in the model system $MgO–Al_2O_3–SiO_2–H_2O$. American Journal of Science, 283, 72–96.

Domanik, K.J., and Holloway, J.R. (1996) The stability and composition of phengitic muscovite and associated phases from 5.5 to 11 GPa: Implications for deeply subducted sediments. Geochimica et Cosmochimica Acta, 60, 4133–4150.

Eggleton, R.A., Boland, J.N., and Ringwood, A.E. (1978) High pressure synthesis of a new aluminium silicate: $Al_5Si_5O_{17}(OH)$. Geochemical Journal, 12, 191–194.

Fockenberg, T. (1998) An experimental study of the pressure-temperature stability of MgMgAl-pumpellyite in the system $MgO-Al_2O_3-SiO_2-H_2O$. American Mineralogist, 83 , 220–227.

Frost, D.J., and Fei, Y. (1998) Stability of phase D at high pressure and high temperature. Journal of Geophysical Research: Solid Earth, 103, 7463–7474.

Gasparik, T. (1993) The role of volatiles in the transition zone. Journal of Geophysical Research: Solid Earth, 98, 4287–4299.

Gemmi, M., Fischer, J., Merlini, M., Poli, S., Fumagalli, P., Mugnaioli, E., and Kolb, U. (2011) A new hydrous Al-bearing pyroxene as a water carrier in subduction zones. Earth and Planetary Science Letters, 310, 422–428.

Gottschalk, M., Fockenberg, T., Grevel, K.-D., Wunder, B., Wirth, R., Schreyer, W., and Maresch, W.V. (2000) Crystal structure of the high-pressure phase $Mg_4(MgAl)Al_4[Si_6O_{21}(OH)_7]$: an analogue of sursassite. European Journal of Mineralogy, 12, 935–945.

Higo, Y., Inoue, T., Irifune, T., and Yurimoto, H. (2001) Effect of water on the spinel-postspinel transformation in Mg_2SiO_4. Geophysical Research Letters, 28, 3505–3508.

Horiuchi, H., Morimoto, N., Yamamoto, K., and Akimoto, S. (1979) Crystal structure of $2Mg_2SiO_4 \cdot 3Mg(OH)_2$, a new high-pressure structure type. American Mineralogist, 64, 593–598.

Inoue, T. (1994) Effect of water on melting phase relations and melt composition in the system Mg_2SiO_4-$MgSiO_3$-H_2O up to 15 GPa. Physics of the Earth and Planetary Interiors, 85, 237–263.

Inoue, T., Yurimoto, H., and Kudoh, Y. (1995) Hydrous modified spinel, $Mg_{1.75}SiH_{0.5}O_4$: A new water reservoir in the mantle transition region. Geophysical Research Letters, 22, 117–120.

Inoue, T., Weidner, D.J., Northrup, P.A., and Parise, J.B. (1998) Elastic properties of hydrous ringwoodite (γ-phase) in Mg_2SiO_4. Earth and Planetary Science Letters, 160, 107–113.

Irifune, T., Kubo, N., Isshiki, M., and Yamasaki, Y. (1998) Phase transformations in serpentine and transportation of water into the lower mantle. Geophysical Research Letters, 25, 203–206.

Kanzaki, M. (1991) Stability of hydrous magnesium silicates in the mantle transition zone. Physics of the Earth and Planetary Interiors, 66, 307–312.

Kirby, S.H., Stein, S., Okal, E.A., and Rubie, D.C. (1996) Metastable mantle phase transformations and deep earthquakes in subducting oceanic lithosphere. Reviews of Geophysics, 34, 261–306.

Komabayashi, T., and Omori, S. (2006) Internally consistent thermodynamic data set for dense hydrous magnesium silicates up to 35 GPa, 1600 °C: Implications for water circulation in the Earth's deep

mantle. Physics of the Earth and Planetary Interiors, 156, 89–107.

Komabayashi, T., Hirose, K., Funakoshi, K., and Takafuji, N. (2005) Stability of phase A in antigorite (serpentine) composition determined by in situ X-ray pressure observations. Physics of the Earth and Planetary Interiors, 151, 276–289.

Kudoh, Y., Finger, L.W., Hazen, R.M., Prewitt, C.T., Kanzaki, M., and Veblen, D.R. (1993) Phase E: A high pressure hydrous silicate with unique crystal chemistry. Physics and Chemistry of Minerals, 19, 357–360.

Kurosawa, M., Yurimoto, H., and Sueno, S. (1997) Patterns in the hydrogen and trace element compositions of mantle olivines. Physics and Chemistry of Minerals, 24, 385–395.

Litasov, K.D., Kagi, H., Shatskiy, A., Ohtani, E., Lakshtanov, D.L., Bass, J.D., and Ito, E. (2007) High hydrogen solubility in Al-rich stishovite and water transport in the lower mantle. Earth and Planetary Science Letters, 262, 620–634.

Liu, L. (1987) Effects of H_2O on the phase behaviour of the forsterite-enstatite system at high pressures and temperatures and implications for the Earth. Physics of the Earth and Planetary Interiors, 49, 142–167.

Mierdel, K., Keppler, H., Smyth, J.R., and Langenhorst, F. (2007) Water solubility in aluminous orthopyroxene and the origin of Earth's asthenosphere. Science, 315, 364.

Miyagi, I., and Yurimoto, H. (1995) Water Content of Melt Inclusions in Phenocrysts Using Secondary

Ion Mass Spectrometer. Bulletin of the Volcanological Society of Japan, 40, 349–355.

Nishi, M., Irifune, T., Tsuchiya, J., Tange, Y., Nishihara, Y., Fujino, K., and Higo, Y. (2014) Stability of hydrous silicate at high pressures and water transport to the deep lower mantle. Nature Geosci, 7, 224–227.

Ohtani, E., Shibata, T., Kubo, T., and Kato, T. (1995) Stability of hydrous phases in the transition zone and the upper most part of the lower mantle. Geophysical Research Letters, 22, 2553–2556.

Ohtani, E., Mizobata, H., Kudoh, Y., Nagase, T., Arashi, H., Yurimoto, H., and Miyagi, I. (1997) A new hydrous silicate, a water reservoir, in the upper part of the lower mantle. Geophysical Research Letters, 24, 1047–1050.

Ohtani, E., Toma, M., Litasov, K., Kubo, T., and Suzuki, a (2001) Stability of dense hydrous magnesium silicate phases and water storage capacity in the transition zone and lower mantle. Physics of the Earth and Planetary Interiors, 124, 105–117.

Okamoto, K., and Maruyama, S. (1999) The high-pressure synthesis of lawsonite in the MORB+H_2O system. American Mineralogist, 84, 362–373.

Pawley, A. (1994) The pressure and temperature stability limits of lawsonite: implications for H_2O recycling in subduction zones. Contributions to Mineralogy and Petrology, 118, 99–108.

Peacock (1990) Fluid processes in subduction zone. Science, 248, 329–337.

Pearson, D.G., Brenker, F.E., Nestola, F., McNeill, J., Nasdala, L., Hutchison, M.T., Matveev, S., Mather,

299 K., Silversmit, G., Schmitz, S., and others (2014) Hydrous mantle transition zone indicated by
300 ringwoodite included within diamond. Nature, 507, 221–4.

301 Rauch, M., and Keppler, H. (2002) Water solubility in orthopyroxene. Contributions to Mineralogy and
302 Petrology, 143, 525–536.

303 Ringwood, A.E., and Major, A. (1967) High-pressure reconnaissance investigations in the system
304 Mg_2SiO_4-MgO-H_2O. Earth and Planetary Science Letters, 2, 130–133.

305 Sakurai, M., Tsujino, N., Sakuma, H., Kawamura, K., and Takahashi, E. (2014) Effects of Al content on
306 water partitioning between orthopyroxene and olivine: Implications for lithosphere–asthenosphere
307 boundary. Earth and Planetary Science Letters, 400, 284–291.

308 Saal, A.E., Hauri, E.H., Langmuir, C.H., and Perfit, M.R. (2002) Vapour undersaturation in primitive
309 mid-ocean-ridge basalt and the volatile content of Earth's upper mantle. Nature, 419, 451–5.

310 Schmidt, M.W., and Poli, S. (1994) The stability of lawsonite and zoisite at high pressures: Experiments
311 in CASH to 92 kbar and implications for the presence of hydrous phases in subducted lithosphere.
312 Earth and Planetary Science Letters, 124, 105–118.

313 Staudigel, H., and Schreyer, W. (1977) The upper thermal stability of clinochlore,
314 $Mg_5Al[AlSi_3O_{10}](OH)_8$, at 10–35 kb P_{H2O}. Contributions to Mineralogy and Petrology, 61,
315 187–198.

316 Suzuki, A., Ohtani, E., and Kamada, T. (2000) A new hydrous phase δ-AlOOH synthesized at 21 GPa
317 and 1000 °C. Physics and Chemistry of Minerals, 27, 689–693.

Wunder, B. (1998) Equilibrium experiments in the system MgO-SiO_2-H_2O (MSH): stability fields of clinohumite-OH [$Mg_9Si_4O_{16}(OH)_2$], chondrodite-OH [$Mg_5Si_2O_8(OH)_2$] and phase A ($Mg_7Si_2O_8(OH)_6$). Contributions to Mineralogy and Petrology, 132, 111–120.

Wunder, B., Rubie, D.C., Ross, C.R., Medenbach, O., Seifert, F., and Schreyer, W. (1993) Synthesis, stability, and properties of $Al_2SiO_4(OH)_2$: a fully dehydrated analogue of topaz. American Mineralogist, 78, 285–297.

Yagi, T., and Akimoto, S. (1976) Direct determination of coesite-stishovite transition by in-situ X-ray measurements. Tectonophysics, 35, 259–270.

Yamamoto, K., and Akimoto, S. (1974) High-pressure and high-temperature investigation in the system MgO-SiO_2-H_2O. Journal of Solid State Chemistry, 9, 187-195.

Yamamoto, K., and Akimoto, S. (1977) The system MgO–SiO_2–H_2O at high pressure and temperatures. Stability field of hydroxyl-chondrodite, hydroxyl-clinohumite and 10 Å phase. American Journal of Science, 277, 288–312.

Figure captions

Figure 1. Cell assembly for high pressure and high temperature experiments. W3%Re-W25%Re thermocouple was used to monitor the temperature.

Figure 2. The chemical composition of the new **23** Å phase in the MAS (+H_2O) ternary diagram. The coexisting phases (pyrope and diaspore, open circles) were also plotted. A: phase A; B: hydrous phase B, super hydrous phase B, anhydrous phase B; D: phase D; E: phase E; Fo: forsterite; Egg: phase egg; Top: topaz-OH; Sp: spinel; Dia: diaspore; Chon: chondrodite; Atg: antigorite; Phg: phengite; Py: pyrope; Chl: Mg-chlorite; Sur: Mg-sursassite; Ctd: chloritoid; Sta: staurolite; Spr: sapphirine; HAPY: hydrous Al-bearing pyroxene; **23** Å: new **23** Å phase in this study.

Fig. 3 Powder X-ray diffraction pattern of the new **23** Å phase $Mg_{11}Al_2Si_4O_{16}(OH)_{12}$. The refined lattice parameters: a = 5.1972(2) Å, c = 22.991(4) Å, and V = 537.8(2) $Å^3$. A: phase A; Br: brucite; Py: pyrope. The solid triangles mark those peaks (at 2θ of about 20.83°, 26.67° and 32.72°) that we cannot identify yet.

Figure 4. The selected-area-electron-diffraction (SAED) patterns (**a**–**e**) and transmission electron image (**f**) of the new **23** Å phase. The SAED patterns were obtained from different grains except for **c** and **d**. The broken lines in **c** and **d** with m indicate a mirror plane perpendicular to the page. **f** shows the stacking fault-like defects.

Figure 5. Stability region of the new **23** Å phase determined in this study. Solid circles represent the presence of the new **23** Å phase, while open circles represent the absence of it. The synthesis condition for HAPY phase (Gemmi et al., 2011) is also shown in solid diamond. The reaction on line (1): New **23** Å phase = Chon + Py + Fo + F; The reaction on line (2): New **23** Å phase = Al-shB + Py + F. The thin dotted line shows the lower pressure limit of phase A (Wunder, 1998), while the thick dotted line indicates the boundary between Chon + Py + Fo + F and Al-shB + Py + F. The phase boundary of coesite-stishovite is from Yagi and Akimoto (1976). The average mantle geotherm (Brown and Shankland, 1981) and the hypothetical P-T paths for the slabs (Kirby et al., 1996; Peacock, 1990) are also shown.

Figure 6. The back-scattered electron image (BEI) of the dehydration products of natural chlorite under 10 GPa and 1000ºC. The new **23** Å phase coexists with pyrope, chondrodite, and phase A. Py, pyrope; phA, phase A; **23** Å, new **23** Å phase in this study; Chon, Chondrodite.

362 Table 1 Chemical compositions of the new **23** Å phase and coexisting phases analyzed by EPMA (EDS

363 or WDS). The compositions of selected standards are also listed.

	S1[a]			S2[a]			Syn[b]		Std[b]	
	Py	Dia	New	Py	Dia	**23** Å	Py	**23** Å	En	Ky
Weight percent										
MgO	31.5(4)	1.0(1)	48.9(7)	31.2(4)	2.0(6)	49.8(9)	30.1(2)	47.4(5)	40.1(5)	0
Al_2O_3	25.6(6)	80.1(9)	11.1(4)	24.9(4)	77.7(6)	11.0(3)	24.2(3)	10.6(2)	0	61.8(4)
SiO_2	43.7(5)	1.0(1)	24.7(4)	44.3(4)	1.5(4)	25.1(4)	44.5(4)	25.7(2)	60.1(9)	37.4(1)
Total	100.8(8)	82.0(9)	84.7(12)	100.4(10)	81.2(9)	85.9(15)	98.8(6)	83.7(4)	100.3(15)	99.2(4)
H_2O[c]	0.26(4)	-	11.2(2)	0.27(4)	-	11.4(2)	-	11.6(2)	-	-
Atomic ratio										
Mg	3.14(3)	0.015(2)	5.65(3)	3.12(2)	0.031(9)	5.68(2)	3.05(3)	5.52(4)	1.00(1)	0
Al	2.02(5)	0.976(3)	1.01(3)	1.96(2)	0.959(10)	0.99(2)	1.94(2)	0.97(2)	0	1.98(1)
Si	2.92(2)	0.010(1)	1.92(2)	2.97(2)	0.015(4)	1.92(2)	3.02(1)	2.01(1)	1.00(1)	1.01(1)
H	0	1	6	0	1	6	0	6	-	-
O	12	2	14	12	2	14	12	14	3	5

Measured by: a, EDS at Ehime University; b, WDS at Ehime University; c, SIMS at Hokkaido University.

- Not determined; Std, standard measurements at the same condition with Syn; Py, pyrope; Dia, diaspore; **23** Å, new **23** Å hydrous phase; En, $MgSiO_3$-enstatite; Ky, kyanite.

364

Tabel 2 The refined X-ray diffraction data of the new **23** Å phase $Mg_{11}Al_2Si_4O_{16}(OH)_{12}$. Main peaks are listed.

hkl	d_{obs}	d_{calc}	I/I_0
0 0 2	11.4782	11.4862	5
0 0 4	5.7368	5.7431	5
0 0 6	3.8259	3.8287	100
1 0 4	3.5358	3.5419	5
0 0 8	2.8696	2.8715	17
1 1 1	2.5797	2.5813	65
1 1 2	2.5323	2.5337	22
1 1 3	2.4589	2.4600	63
1 0 8	2.4205	2.4206	4
0 0 10	2.2969	2.2972	14
1 1 6	2.1488	2.1496	55
1 1 7	2.0364	2.0368	52
1 1 8	1.9265	1.9264	40
1 1 9	1.8205	1.8207	3
2 0 8	1.7707	1.7709	4
2 1 0	1.7003	1.7006	8
2 1 1	1.6969	1.6960	5
2 1 4	1.6303	1.6306	13
1 1 11	1.6278	1.6276	10
1 0 14	1.5420	1.5416	14
3 0 0	1.5006	1.4998	95
3 0 6	1.3964	1.3965	12
1 1 14	1.3880	1.3873	18
1 1 15	1.3198	1.3193	7

370 **Fig. 1** Cell assembly for high pressure and high temperature experiments. W3%Re-W25%Re
371 thermocouple was used to monitor the temperature.

372

373 **Fig. 2** The chemical composition of the new **23** Å phase in the MAS (+H_2O) ternary diagram. The
374 coexisting phases (pyrope and diaspore, open circles) were also plotted. A: phase A; B: hydrous phase B,
375 super hydrous phase B, anhydrous phase B; D: phase D; E: phase E; Fo: forsterite; Egg: phase egg; Top:
376 topaz-OH; Sp: spinel; Dia: diaspore; Chon: chondrodite; Atg: antigorite; Phg: phengite; Py: pyrope; Chl:
377 Mg-chlorite; Sur: Mg-sursassite; Ctd: chloritoid; Sta: staurolite; Spr: sapphirine; HAPY: hydrous
378 Al-bearing pyroxene; **23** Å: new **23** Å phase in this study.

379

380 **Fig. 3**. Powder X-ray diffraction pattern of the new 23Å phase Mg11Al2Si4O16(OH)12. The refined
381 lattice parameters: a = 5.1972(2) Å, c = 22.991(4) Å, and V = 537.8(2) $Å^3$. A: phase A; Br: brucite; Py:
382 pyrope. The solid triangles mark those peaks (at 2□ of about 20.83°, 26.67° and 32.72°) that we cannot
383 identify yet.

384

385 **Fig. 4** The selected-area-electron-diffraction (SAED) patterns (**a**–**e**) and transmission electron image (**f**)
386 of the new **23** Å phase. The SAED patterns were obtained from different grains except for **c** and **d**. The

broken lines in **c** and **d** with m indicate a mirror plane perpendicular to the page. **f** shows the stacking fault-like defects.

Fig. 5 Stability region of the new **23** Å phase determined in this study. Solid circles represent the presence of the new **23** Å phase, while open circles represent the absence of it. The synthesis condition for HAPY phase (Gemmi et al., 2011) is also shown in solid diamond. The reaction on line (1): New **23** Å phase = Chon + Py + Fo + F; The reaction on line (2): New **23** Å phase = Al-shB + Py + F. The thin dotted line shows the lower pressure limit of phase A (Wunder, 1998), while the thick dotted line indicates the boundary between Chon + Py + Fo + F and Al-shB + Py + F. The phase boundary of coesite-stishovite is from Yagi and Akimoto (1976). The average mantle geotherm (Brown and Shankland, 1981) and the hypothetical P-T paths for the slabs (Kirby et al., 1996; Peacock, 1990) are also shown.

Fig. 6 The back-scattered electron image (BEI) of the dehydration products of natural chlorite under 10 GPa and 1000 ºC. The new **23** Å phase coexists with pyrope, chondrodite, and phase A. Py, pyrope; phA, phase A; **23** Å, new **23** Å phase in this study; Chon, chondrodite.

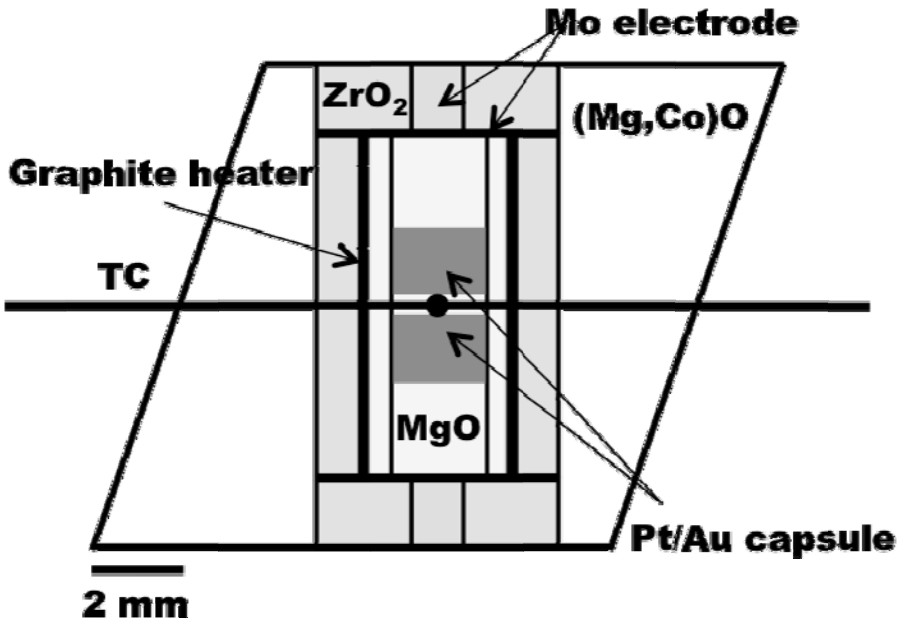

368

370 **Fig. 1** Cell assembly for high pressure and high temperature experiments. W3%Re-W25%Re

371 thermocouple was used to monitor the temperature.

371

372 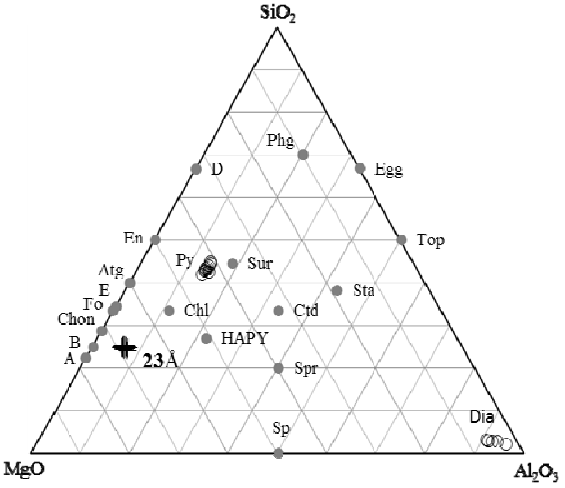

379 **Fig. 2** The chemical composition of the new phase in the MAS (+H_2O) ternary diagram.
380 The coexisting phases (pyrope and diaspore, open circles) were also plotted. A: phase A; B:
381 hydrous phase B, super hydrous phase B, anhydrous phase B; D: phase D; E: phase E; Fo:
382 forsterite; Egg: phase egg; Top: topaz-OH; Sp: spinel; Dia: diaspore; Chon: chondrodite;
383 Atg: antigorite; Phg: phengite; Py: pyrope; Chl: Mg-chlorite; Sur: Mg-sursassite; Ctd:
384 chloritoid; Sta: staurolite; Spr: sapphirine; HAPY: hydrous Al-bearing pyroxene; **23** Å: new
385 **23** Å phase in this study.

380

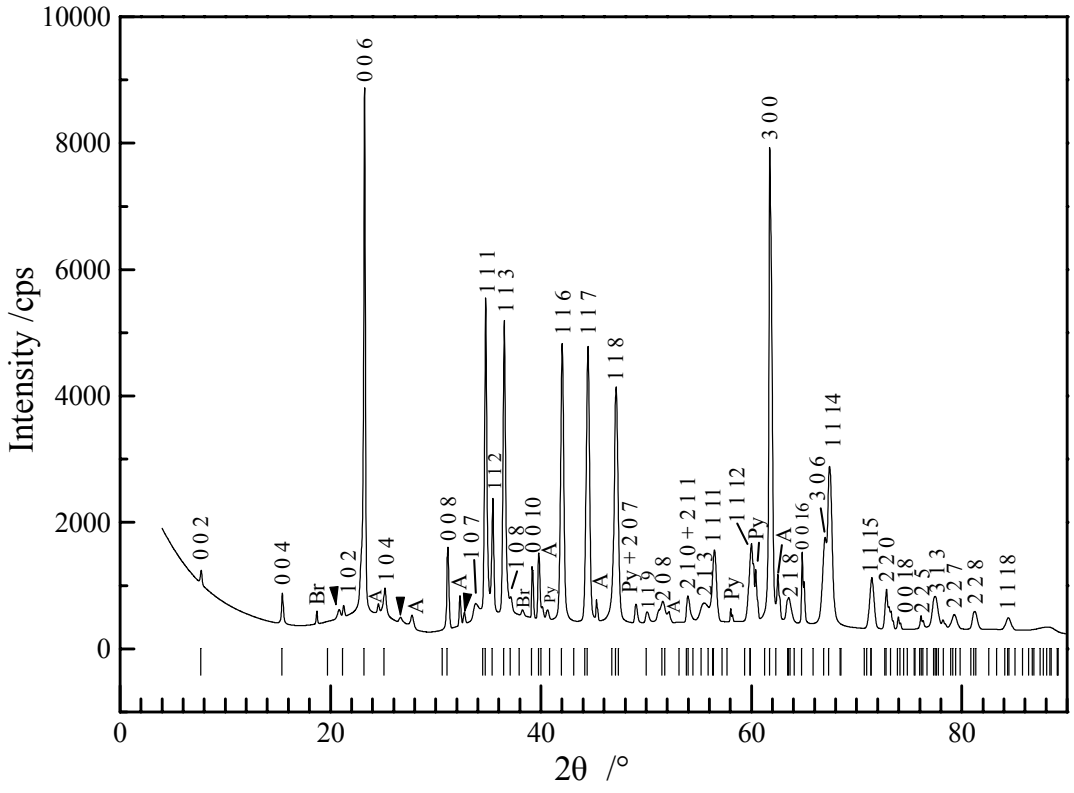

380

381 **Fig. 3** Powder X-ray diffraction pattern of the new **23** Å phase $Mg_{11}Al_2Si_4O_{16}(OH)_{12}$. The refined lattice

382 parameters: a = 5.1972(2) Å, c = 22.991(4) Å, and V = 537.8(2) Å^3. A: phase A; Br: brucite; Py: pyrope.

383 The solid triangles mark those peaks (at 2θ of about 20.83°, 26.67° and 32.72°) that we cannot identify

384 yet.

385

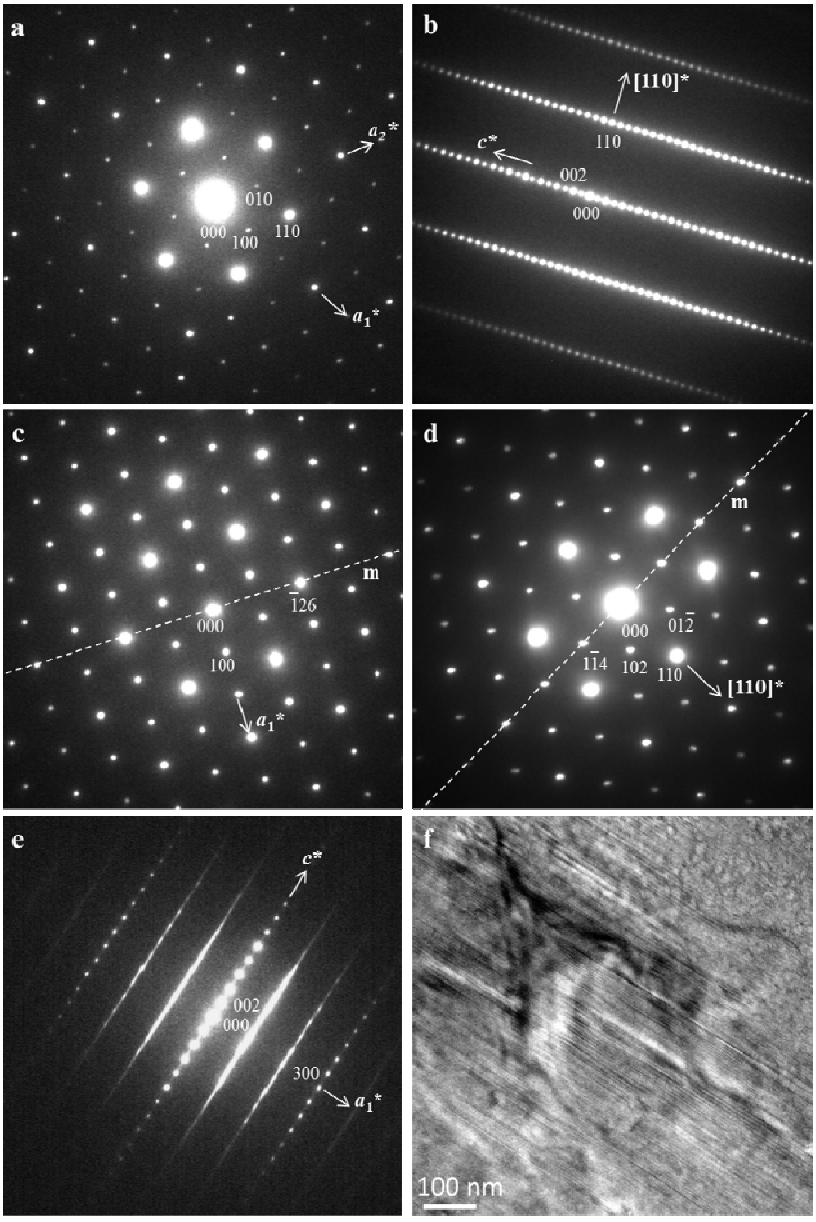

387

391 **Fig. 4** The selected-area-electron-diffraction (SAED) patterns (**a**–**e**) and transmission electron image (**f**)

392 of the new **23** Å phase. The SAED patterns were obtained from different grains except for **c** and **d**. The

393 broken lines in **c** and **d** with m indicate a mirror plane perpendicular to the page. **f** shows the stacking

394 fault-like defects.

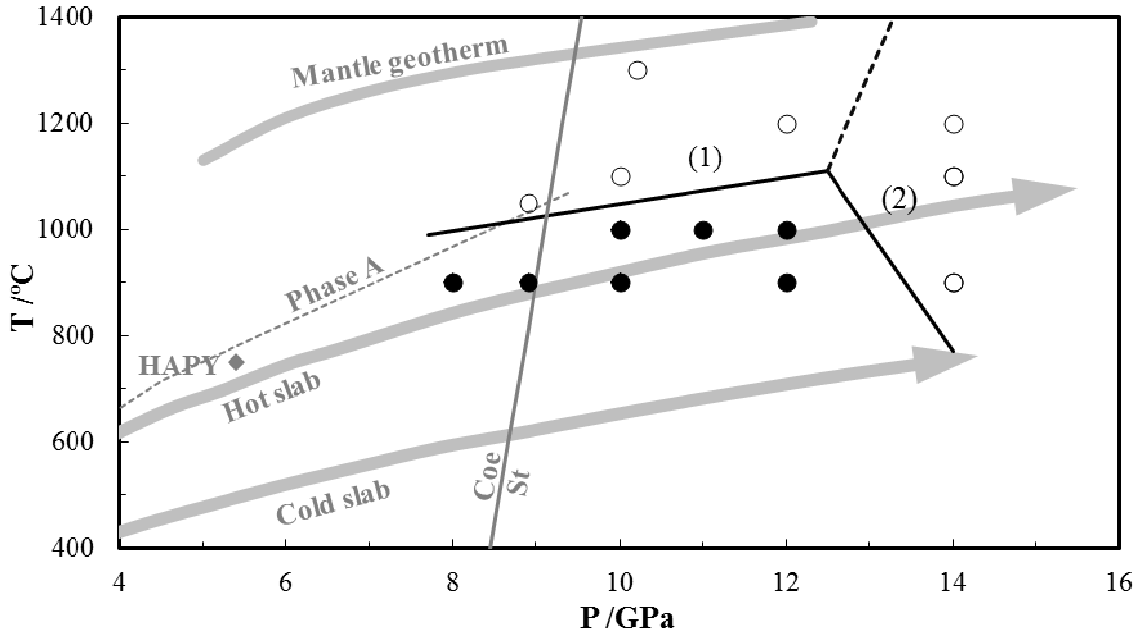

392

391 **Fig. 5** Stability region of the new **23** Å phase determined in this study. Solid circles represent the

392 presence of the new **23** Å phase, while open circles represent the absence of it. The synthesis condition

393 for HAPY phase (Gemmi et al., 2011) is also shown in solid diamond. The reaction on line (1): New **23**

394 Å phase = Chon + Py + Fo + F; The reaction on line (2): New **23** Å phase = Al-shB + Py + F. The thin

395 dotted line shows the lower pressure limit of phase A (Wunder, 1998), while the thick dotted line

396 indicates the boundary between Chon + Py + Fo + F and Al-shB + Py + F. The phase boundary of

397 coesite-stishovite is from Yagi and Akimoto (1976). The average mantle geotherm (Brown and

398 Shankland, 1981) and the hypothetical P-T paths for the slabs (Kirby et al., 1996; Peacock, 1990) are

409 also shown.

402

403

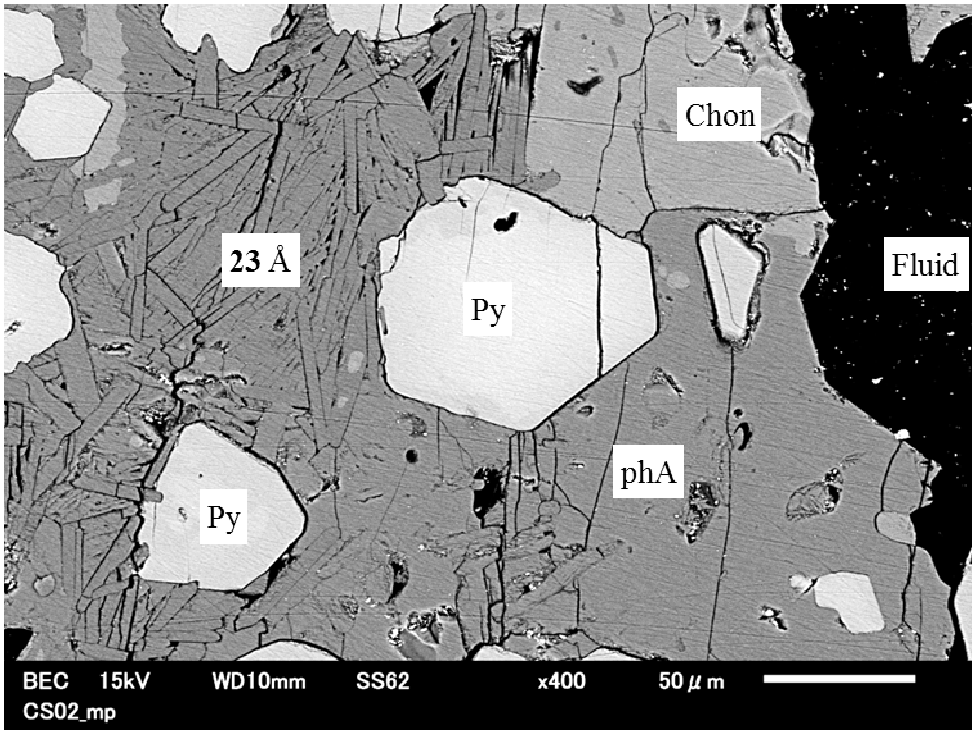

404

407 **Fig. 6** The back-scattered electron image (BEI) of the dehydration products of natural chlorite under 10

408 GPa and 1000 ºC. The new **23** Å phase coexists with pyrope, chondrodite, and phase A. Py, pyrope; phA,

409 phase A; **23** Å, new **23** Å phase in this study; Chon, chondrodite.

408